International Journal of Heat and Mass Transfer 219 (2024) 124827

Contents lists available at ScienceDirect

International Journal of Heat and Mass Transfer

journal homepage: www.elsevier.com/locate/ijhmt

Heat transfer modification in an unsteady laminar boundary layer subject to free-stream traveling waves

Tapish Agarwal, Beni Cukurel, Ian Jacobi *

Faculty of Aerospace Engineering, Technion Israel Institute of Technology, Haifa, 32000, Israel

A B S T R A C T

A laminar, thermal boundary layer was forced computationally by free-stream, traveling-wave velocity fluctuations and the effects on the wall heat flux and skin friction were measured as a function of the phase speed of the disturbances and the streamwise location along the developing flow. The heat flux modification due to the flow forcing was significantly higher than the corresponding skin friction enhancement, and the dependence of these two transport properties on the phase speed was qualitatively different. The skin friction modification exhibited a maximum at an optimal phase speed, which was explained in terms of the overlap of two distinct viscous layers within the boundary layer. The heat flux modification did not exhibit this maximum, although evidence was found to suggest such a maximum may occur with sufficient boundary layer development. Because the magnitude of the wall heat-flux modification scales quadratically with wave amplitude, traveling wave disturbances pose significant challenges for thermal transport measurements in periodically perturbed environments, like turbomachinery, but also new opportunities for the control of heat transfer.

1. Introduction

The control of fluid flow and associated transport processes provides an avenue to increase efficiencies of various thermo-fluid systems. Flow control strategies have been developed to decrease the skin friction using passive [19] and active [4,14,31] methods, and to increase the heat transfer for a variety of heat exchange applications [9]. The turbine environment provides a particularly challenging and important case in which modifying skin friction and thermal fluxes can have a significant impact on the overall design of turbine blades and thus the overall efficiency of turbomachinery [36]. And turbines pose unique challenges to flow and heat transfer measurement and modification due to the natural unsteadiness and periodic perturbations present in their operation. These natural flow fluctuations result from vortex shedding, the unsteady wakes of engine components, and the blade passing frequency between stator/turbine stages, and have been shown to affect skin friction and heat transfer on turbine blades significantly [10,29,35]. Ameri et al. [3] reported a variation in heat transfer of as much as 8% on the suction side and 20% on the pressure side of turbine blades due to unsteady wakes; similar trends were observed by Jiang et al. [16]. These large variations of heat transfer due to unsteady fluid phenomenon in the turbine blade pose a serious challenge for the design of turbine blades and cooling systems (including flow rates, placement, size of cooling holes).

In order to develop effective control strategies in these unsteady environments, the effect of unsteady flow perturbations on the transport properties of the system must first be explained. Many of these flow perturbations take the form of free-stream traveling waves, as time-varying vortices are shed and convect downstream where they influence the nearby, developing boundary layers, although some perturbations can be modeled more simply as purely temporal waves or standing waves [30].

The response of boundary layers to free stream perturbations has received considerable attention, in both laminar and turbulent boundary layers, although most of these studies have focused on the momentum transfer [20,22,1,24], with only a few studies reporting heat transfer modifications.

1.1. Free-stream wave effects on momentum transport

Free-stream disturbances can induce significant velocity fluctuations within the boundary layer. The classical studies of these induced fluctuations have focused on wavy, free-stream disturbances, characterized (in general) by angular frequency $\hat{\omega}$, wavelength, $\hat{\lambda}$, phase-speed, $\hat{c}$ (dimensional quantities are denoted by the hat) and non-dimensional amplitude, ε, defined with respect to the free-stream velocity scale, $\hat{U}$.

Hill and Stenning [13] studied the case of purely temporal, free-stream oscillations for Blasius and Howarth flows. They found the amplitude and phase of the streamwise fluctuations induced within the

* Corresponding author.
E-mail address: ijacobi@technion.ac.il (I. Jacobi).

https://doi.org/10.1016/j.ijheatmasstransfer.2023.124827
Received 21 July 2023; Received in revised form 1 October 2023; Accepted 13 October 2023

Nomenclature

Dimensionless Numbers

Ec	Eckert Number
Re	Reynolds number, $\hat{U}\hat{\ell}/\hat{\nu}$
Re_1	Streaming Reynolds number, $\hat{U}^2/\hat{\nu}\hat{\omega}$
St	Strouhal Number, $\hat{\omega}\hat{\ell}/\hat{U}$
St_x	Strouhal Number based on stream-wise distance, $\hat{\omega}\hat{x}/\hat{U}$
ε	amplitude of fluctuations, $\hat{u}_1/\hat{U}$
C_f	Skin friction coefficient
C_p	Coefficient of static pressure
h_f	Coefficient of heat transfer
Pr	Prandtl number, $\hat{\nu}/\hat{\alpha}$

Greek Alphabet

α_c	Velocity profile approximation constant
α_s	Stokes layer overshoot constant
ρ	Fluid density
Θ	Temperature
α	Thermal diffusivity
Λ	Thermal Conductivity
λ	Wavelength
μ	Dynamic viscosity
ν	Kinematic viscosity
ω	Angular frequency of oscillations

Latin Alphabet

ℓ	Characteristic length scale
f	Non-linear forcing
p	Static pressure
t	Time
u	Stream-wise velocity
v	Wall-normal velocity
x	Stream-wise coordinate
y	Wall normal coordinate
y_c	Location of critical layer
y_s	Location of Stokes layer
c_p	Isobaric specific heat capacity
C	Airfoil chord
c	Wave Speed, ω/k
k	Wave number
H	Channel half-height
U	Steady velocity at the free stream

Subscripts and Superscripts

$\hat{q}$	Dimensional quantities
$\overline{q}$	Time Averaged quantities
q'	Fluctuating quantities
q_0	Unforced case
q_1	Imposed quantities
q_∞	Free stream quantities
q_Θ	Thermal quantities
q_w	Wall quantities
q	Non-dimensional quantities

boundary layer vary with forcing frequency and the stream-wise position inside the boundary layer, $\hat{x}$, which they collapsed to a Strouhal number, $\mathrm{St}_x = \frac{\hat{\omega}\hat{x}}{\hat{U}}$. The near-wall amplification of stream-wise fluctuations was found to be negligible at high St_x and as much as 20% for low St_x. The phase of stream-wise fluctuations was found to lead the free-stream forcing by about +45° at the wall, then declining to −10° moving away from the wall, until finally aligning with the forcing at the outer-edge of the boundary layer. For temporal wave forcing, the spatial region over which these amplitude and phase changes occur is known as the Stokes' layer, in analogy to Stokes' second problem (but with the addition of a free-stream flow). The height of the Stokes layer above the wall, $\hat{y}_s$, is given in terms of the angular frequency and the kinematic viscosity of the fluid, $\hat{\nu}$, as $\hat{y}_s \sim \sqrt{\hat{\nu}/\hat{\omega}}$.

Patel [24] studied traveling wave forcing by inserting a flapping plate upstream of the developing laminar boundary layer, to generate waves with a phase-speed, $\hat{c} = 0.77\hat{U}$ (later corrected to $0.66\hat{U}$ by Evans [8]). The stream-wise velocity fluctuations in the boundary layer exhibited much larger amplification than in the case of temporal waves, and a greater phase lag near the wall on the order of +120°. (Patel and Young [25] reported similar amplitude and phase trends for the same experiment in a turbulent boundary layer.)

All of the above studies focused only on the velocity fluctuations but did not examine the effect of the free-stream forcing on the mean velocity profile. Although the time averaged contribution of such forcing on the mean flow is generally small, it can exert a significant impact on the skin friction coefficient, C_f in certain cases, via the non-linear interaction between the velocity fluctuations and the viscous shear that is referred to as steady streaming. A modern review of steady streaming can be found in Riley [26], with the classical treatment discussed in Telionis [33]. The structure of streaming layers is reviewed in Stuart [32]. Telionis and Romaniuk [34] calculated steady streaming effects on both skin friction and heat transfer for temporal oscillations of varying frequency and showed that the effect of streaming was significant for some intermediate values of frequencies. Choi extended these streaming calculations for traveling and standing waves for momentum transport, and found a much stronger response [7,5,6], indicating that the traveling wave effects may dominate over other sources of flow perturbation, consistent with the results of Patel [24].

The reason traveling waves exert such a strong effect on momentum transport is due to the presence of a second viscous layer, in addition to the Stokes layer that is generated for temporal oscillatings. This second viscous layer is known as the critical layer and is the result of viscosity smoothing out a singularity in the inviscid Rayleigh equation [28]. The momentum streaming implications of the critical layer have been explored only recently by Hoepffner and Fukagata [15] and Mamori et al. [21]. In Agarwal et al. [2], we analyzed the structure of the critical layer to predict the effect of traveling waves on skin friction modification in a laminar boundary layer. Specifically, we developed a heuristic model to identify the optimal phase-speed of traveling waves at a given streamwise position to locally modify the skin friction by generating an overlap between the critical and Stokes layers; this concept will be revisited below in §3.1 as part of the current study.

1.2. Traveling wave effects on thermal transport

Despite the significance of traveling wave disturbances on momentum transport, their effect on heat transport has not received much attention. Hasegawa performed a series of studies on both momentum and thermal transport in channel flows using traveling-wave wall suction and blowing [11,17,18], and a similar study was reported by Higashi et al. [12]. Higashi et al. [12] observed different effects on the skin friction versus the heat transfer and ascribed these differences to the opposing phases of velocity and temperature fluctuations. Kaithakkal et al. [18] reported similar differences and explained them in terms of the differences between the Reynolds shear stress and convective heat flux. But, unlike the classic studies on free-stream forcing, these studies all utilized wall-forcing to generate wavy slip and penetration conditions in order to force the flow. And these studies focused on fully developed channel flows, in both the laminar and turbulent regimes, instead of the classical laminar boundary layer.

Despite the differences, these studies identified the importance of critical layer enhancement of both momentum and thermal transport, and they reported an optimal phase speed for the traveling wave disturbances at which this critical layer enhancement was maximized. However, they did not explain the value of this optimal phase speed, nor did they connect the critical layer phenomena to the differences observed between the momentum and thermal transport modifications. These pioneering works therefore left a number of important questions open for further investigation. The fact that their channel geometry differed from the classic boundary layer studies also makes direct comparisons with the earlier studies more challenging. Therefore, in order to further explore the heat flux enhancement via traveling wave forcing, we returned to the classical case of the laminar boundary layer with free-stream forcing.

1.3. Outline

In this study, we build on our previous study of skin friction enhancement and apply it to the problem of heat flux enhancement in a laminar boundary layer, with comparisons to both momentum transport in the boundary layer and heat transport in the forced channel flow. In §2, we describe the equations governing the mean and fluctuating momentum and temperature over a laminar boundary layer. In §3.1, we review the skin friction modification behavior and contrast it with the heat transfer modification, and we note that the wall heat flux does not appear to exhibit an optimal phase speed. We explore the existence of an optimal phase speed for momentum and heat fluxes in §3.2 and 3.3 and provide possible rationales for its apparent absence in the developing boundary layer, as compared to the channel flow. Finally, we report on the Prandtl number scaling behavior of thermal streaming in §3.4.

2. Laminar boundary layer model

Following the study of Agarwal et al. [2] for the momentum boundary layer, we adopt the approach of Lin [20] to calculate the thermal boundary layer response to traveling waves via a Reynolds decomposition of the flow quantities and a coupled, iterative solution of the mean and fluctuating flow fields.

The two-dimensional equations governing momentum and thermal transport were derived following [27], assuming constant thermal conductivity $\hat{\Lambda}$, isobaric specific heat capacity $\hat{c}_p$, density $\hat{\rho}$, and dynamic viscosity, $\hat{\mu}$. The velocity, $(\hat{u},\hat{v})$, and temperature, $\hat{\Theta}$, fields were non-dimensionalized as $(u,v,\Theta)=(\hat{u}/\hat{U},\hat{v}/\hat{U},(\hat{\Theta}-\hat{\Theta}_w)/(\hat{\Theta}_\infty-\hat{\Theta}_w))$, where $\hat{\Theta}_w$ is the wall temperature and $\hat{\Theta}_\infty$ is the free stream temperature. The coordinates were non-dimensionalized as $(x,y,t)=(\hat{x}/\hat{\ell},\hat{y}/\hat{\ell},\hat{t}\hat{\omega})$, where $\hat{\ell}$ is a characteristic wall-normal length scale. We then adopted an inertial scaling

$$(u,v,\Theta,X,Y,T)=(u,v,\Theta,x\mathrm{Re},y\mathrm{Re},t\mathrm{Re}/\mathrm{St}), \tag{1}$$

where the Reynolds number is given by $\mathrm{Re}=\frac{\hat{U}\hat{\ell}}{\hat{\nu}}$ and the Strouhal number by $\mathrm{St}=\frac{\hat{\omega}\hat{\ell}}{\hat{U}}$. The resulting instantaneous dynamics are

$$\frac{\partial u}{\partial T}+u\frac{\partial u}{\partial X}+v\frac{\partial u}{\partial Y}=-\frac{\partial p}{\partial X}+\frac{\partial^2 u}{\partial Y^2},\qquad v(X,Y)=-\int_0^Y\frac{\partial}{\partial X}u(X,s)\,ds \tag{2}$$

$$\frac{\partial\Theta}{\partial T}+u\frac{\partial\Theta}{\partial X}+v\frac{\partial\Theta}{\partial Y}=\frac{1}{\mathrm{Pr}}\left(\frac{\partial^2\Theta}{\partial X^2}+\frac{\partial^2\Theta}{\partial Y^2}\right)+2\,\mathrm{Ec}\left[\left(\frac{\partial u}{\partial X}\right)^2+\left(\frac{\partial v}{\partial Y}\right)^2\right]+\mathrm{Ec}\left(\frac{\partial v}{\partial X}+\frac{\partial u}{\partial Y}\right)^2 \tag{3}$$

where the Prandtl Number was defined as $\mathrm{Pr}=\frac{\hat{\nu}\hat{\rho}\hat{c}_p}{\hat{\Lambda}}$, and Eckert Number as $\mathrm{Ec}=\frac{\hat{U}^2}{\hat{c}_p(\hat{\Theta}_\infty-\hat{\Theta}_w)}$.

Flow quantities were decomposed into mean $(\overline{q})$ and fluctuating (q') quantities. Imposing the boundary layer assumptions and neglecting Ec (because of negligible dissipation), we write the mean dynamics as:

$$\bar{u}\frac{\partial\bar{u}}{\partial X}+\bar{v}\frac{\partial\bar{u}}{\partial Y}=\frac{\partial^2\bar{u}}{\partial Y^2}+\varepsilon^2\underbrace{\overline{\left(-u'\frac{\partial u'}{\partial X}-v'\frac{\partial u'}{\partial Y}\right)}}_{f(X,Y)},$$

$$\bar{v}(X,Y)=-\int_0^Y\frac{\partial}{\partial X}\bar{u}(X,s)\,ds \tag{4}$$

$$\bar{u}\frac{\partial\overline{\Theta}}{\partial X}+\bar{v}\frac{\partial\overline{\Theta}}{\partial Y}=\frac{1}{\mathrm{Pr}}\left(\frac{\partial^2\overline{\Theta}}{\partial Y^2}\right)+\varepsilon^2\underbrace{\overline{\left(-u'\frac{\partial\Theta'}{\partial X}-v'\frac{\partial\Theta'}{\partial Y}\right)}}_{f_\Theta(X,Y)} \tag{5}$$

where $f(X,Y)$ and $f_\Theta(X,Y)$ are the net forcing to the mean momentum and thermal transport equations, respectively. Momentum forcing is a result of non-linear interactions between components of velocity fluctuations (i.e. Reynolds stresses), and thermal forcing is a result of interactions between temperature and velocity fluctuations.

Similarly, the fluctuating dynamics were written as:

$$\frac{\partial u'}{\partial T}-\frac{\partial^2 u'}{\partial Y^2}-\frac{\partial u_1}{\partial T}=\left(\frac{\partial u_1}{\partial X}-\bar{u}\frac{\partial u'}{\partial X}-\bar{v}\frac{\partial u'}{\partial Y}\right)+\left(-u'\frac{\partial\bar{u}}{\partial X}-v'\frac{\partial\bar{u}}{\partial Y}\right)+\varepsilon\left\{\left(u_1\frac{\partial u_1}{\partial X}-u'\frac{\partial u'}{\partial X}-v'\frac{\partial u'}{\partial Y}\right)-f(X,Y)\right\},$$

$$v'(X,Y)=-\int_0^Y\frac{\partial}{\partial X}u'(X,s)\,ds, \tag{6}$$

$$\frac{\partial\Theta'}{\partial T}-\frac{1}{\mathrm{Pr}}\left(\frac{\partial^2\Theta'}{\partial Y^2}\right)=\left(-\bar{u}\frac{\partial\Theta'}{\partial X}-\bar{v}\frac{\partial\Theta'}{\partial Y}\right)+\left(-u'\frac{\partial\overline{\Theta}}{\partial X}-v'\frac{\partial\overline{\Theta}}{\partial Y}\right)+\varepsilon\left\{\left(-u'\frac{\partial\Theta'}{\partial X}-v'\frac{\partial\Theta'}{\partial Y}\right)-f_\Theta(X,Y)\right\} \tag{7}$$

where the free stream pressure gradient was written in terms of the free stream velocity perturbation, denoted $u_1=u_1\left[|c\mathrm{Re}_1|^{-1}(X-cT)\right]$, where u_1 is a periodic function, in this case taken as sine. The boundary conditions for the momentum and thermal transport equations enforced no-slip and constant temperature conditions at the wall and fixed free-stream velocities and temperatures, according to:

$$\begin{aligned}&(X,Y=0):\quad u'=v'=\Theta'=\bar{u}=\bar{v}=\bar{\Theta}=0\\&(X=0,Y):\quad u'=u_1(-\mathrm{Re}_1^{-1}T),v'=\Theta'=0,\bar{u}=\bar{\Theta}=1,\bar{v}=0\\&(X,Y\to\infty):\quad \bar{u}=\bar{\Theta}=1\end{aligned} \tag{8}$$

where the streaming Reynolds number, $\mathrm{Re}_1=\frac{\hat{U}^2}{\hat{\omega}\hat{\nu}}$, represents the frequency of the traveling wave perturbation in the free-stream.

The above system of equations describes the developing boundary layer illustrated in Fig. 1. The system was solved on a rectangular domain with a uniformly spaced grid using a predictor/corrector approach. First, the mean momentum dynamics equation (4) was solved while neglecting the momentum forcing, $f(X,Y)$. The solution from that was used to solve the fluctuating momentum dynamics, equation (6), which was then used to make a first estimate of the momentum forcing, $f(X,Y)$. The mean momentum equation (4) solution was then updated, taking into account the forcing estimate. The new mean solution was then used to make the next estimate of fluctuating flow. This process was repeated until a converged mean flow was obtained. The converged mean and fluctuating velocity components were then used as inputs to the heat equations, (5) and (7), which were solved iteratively following the same approach. Converged solutions could not be obtained for very high Reynolds numbers, due to numerical instabilities, and those few points are indicated in gray in the colormaps presented in §3. Details about the solution procedure and the numerical methods are described in Agarwal et al. [2].

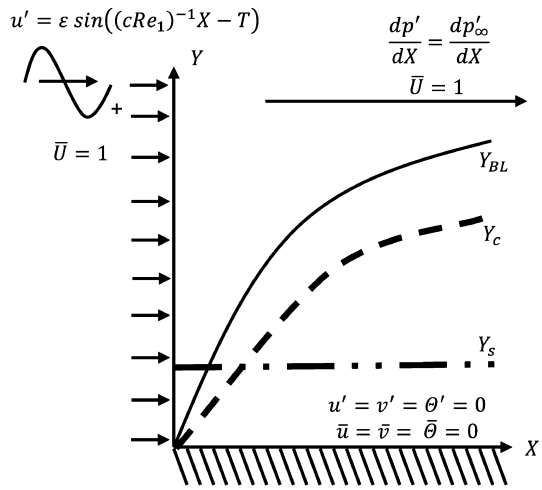

Fig. 1. Setup of the problem, showing the rectangular domain, the boundary conditions at the inlet, wall and free stream, and the three viscous layers: boundary layer, Y_{BL}, critical layer, Y_c, and Stokes layer, Y_s.

The solution to these equations provides the mean and fluctuating values of the velocity and temperature, which are then used to calculate the skin friction and heat transfer coefficients, which appear in non-dimensional form as $\overline{C}_f = \frac{\partial \bar{u}}{\partial Y}\Big|_{Y=0}$ and $\overline{h}_f = -\frac{\partial \bar{\Theta}}{\partial Y}\Big|_{Y=0}$.

3. Results and discussion

3.1. Mean skin friction and heat flux modification

The relative change in skin friction coefficient between the forced and unforced boundary layers is defined as $\frac{\Delta C_f}{C_{f0}} = \frac{C_f - C_{f0}}{C_{f0}}$, where, C_f and C_{f0} are the skin friction coefficients for forced and unforced cases, respectively. $\frac{\Delta C_f}{C_{f0}}$, is shown as a function of Reynolds number based on streamwise location, X (where $\mathrm{Re} \sim X^{1/2}$), and inverse phase speed, c^{-1}, in Fig. 2. Upstream traveling waves, $c^{-1} < 0$, result in a decrease in skin friction, the magnitude of which increases with Reynolds number and decreases with phase speed. The impact of sub-critical downstream traveling waves, $0 < c^{-1} \leq 1$, on skin friction is insignificant. Critical waves, $c^{-1} > 1$, impact the skin friction in a significant manner, including both large increases and decreases in the skin friction. In Agarwal et al. [2], it was observed that the region of increased skin friction in the upper right of the figure corresponds to the overlap of Stokes and critical layers, marked in the solid black line and discussed further in §3.2.

Like the skin friction, the relative change in the heat transfer coefficient at the wall was defined as $\frac{\Delta h_f}{h_{f0}} = \frac{h_f - h_{f0}}{h_{f0}}$ where, h_f and h_{f0} are the heat transfer coefficients for forced and unforced cases, respectively. $\frac{\Delta h_f}{h_{f0}}$ as a function of X and c^{-1} is shown in Fig. 3. Upstream traveling waves result in a small decrease in heat transfer, the magnitude of which increases with Reynolds number and decreases with phase speed. Downstream traveling critical waves result in a large increase in heat transfer, which apparently increases monotonically with Reynolds number and decreases with phase speed. For a forcing amplitude of $\varepsilon = 1\%$, the maximum increase in relative heat flux is of the order of 12%, which is much larger than corresponding relative skin friction increase of 4%.

The skin friction and heat flux modifications were found to scale with ε^2. Thus, larger amplitude fluctuations will result in quadratically larger modifications in the quantities of interest. The streaming Reynolds number, Re_1, only stretches the flux modifications in the stream-wise direction. Thus, changes in skin friction and heat transfer modifications can be absorbed by scaling the Reynolds number X with

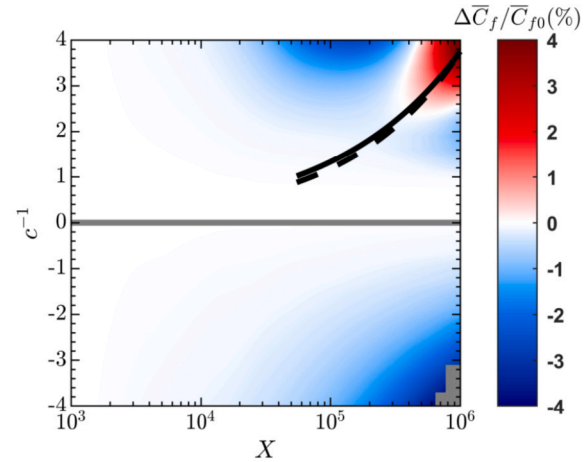

Fig. 2. Relative change in skin friction as a function of Reynolds number (X) and inverse phase speed (c^{-1}), for (ε, Re_1, Pr) = (0.01, 2×10^4, 0.71). The solid black line depicts the empirical intersection of the Stokes layer and critical point; the dashed line is a heuristic model of this intersection developed in equation (11) with $\alpha_s = 4\sqrt{2}$ and fitted coefficient $\alpha_c \approx 1/3$. The gray points denote unconverged velocity fields as noted in §2.

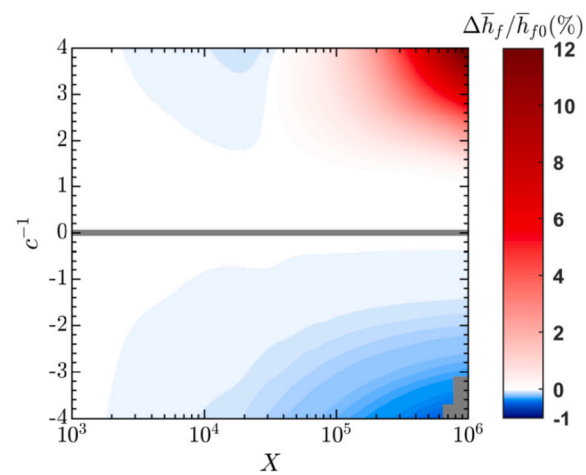

Fig. 3. Relative change in heat transfer coefficient, as a function of Reynolds number (X) and inverse phase speed (c^{-1}), for (ε, Re_1, Pr) = (0.01, 2×10^4, 0.71).

the streaming Reynolds number, Re_1, resulting in the Strouhal number scaling, $\mathrm{St}_x = X/\mathrm{Re}_1$, that was first used in Hill and Stenning [13].

In addition to the stronger overall effect of traveling wave perturbations on heat flux versus its effect on skin friction, it is important to emphasize that the pattern in that modification as a function of Reynolds number and phase speed is also vastly different when we compare the heat flux modification in Fig. 3 and the skin friction modification in Fig. 2. There does not appear to be an optimal phase speed at which the heat transfer is maximized for a given Reynolds number, as there was for the skin friction. To explain this difference, it is first useful to reconsider the origins of the optimal phase speed for skin friction and see what is different for the case of heat transfer.

3.2. Optimal phase speed for skin friction enhancement

Fig. 2 reveals that the region of optimal skin friction modification in the downstream traveling waves (in the upper right corner) occurs in the vicinity of particular pairs of phase speeds and Reynolds numbers. In our previous study on skin friction enhancement, we argued that the maximal amplification of wall transport occurs for traveling waves whose phase speed, c, matches the mean velocity profile, $u(Y)$,

i.e. $u(Y_c) = c$, at the location of the Stokes layer, Y_s [2]. In other words, maximal amplification occurs where the critical layer and Stokes layers overlap for a given wave,

$$Y_c = Y_s \tag{9}$$

This overlap resulted in a phase coherence between the different velocity components interacting non-linearly in the forcing term, $f(X, Y)$, which resulted in a significant magnification of the forcing and thus a modification of the mean velocity gradient.

In a generalization of the empirical results reported in Agarwal et al. [2], we show here that the optimal phase speed can be predicted by writing this overlap argument in terms of the approximate size of the Stokes layer and shape of the velocity profile. The overshoot location of the Stokes layer is described by $Y_s = \alpha_s \sqrt{Re_1}$, where $\alpha_s = 4\sqrt{2}$. For the laminar boundary layer case, we assume the Blasius profile is nearly linear near the wall and that the Stokes layer falls within this approximately linear region (based on Schlichting [27] or via the series approximation of Blasius):

$$u = \alpha_c \left(\frac{Y}{\sqrt{X}} \right) \tag{10}$$

where α_c is a non-dimensional fitting factor of $\mathcal{O}(1)$. At the critical layer location, $u(Y_c) = c$, we can invert the linear velocity profile and equate its wall-normal location, Y_c, with that of the Stokes layer, Y_s, to obtain

$$Re_1 \left(c^{-1}\right)^2 = \frac{1}{\alpha_c^2 \alpha_s^2} X \approx \frac{9}{32} X \tag{11}$$

where $\alpha_c \approx 1/3$ by fitting. This functional relationship is shown as the dashed line in Fig. 2, which nearly overlaps the solid line representing the empirical intersection of the Stokes and critical layers. The simple, heuristic result compares quite well with the quasi-empirical relation that we previously reported in Agarwal et al. [2]:

$$\mathrm{Re}_1^{10/9} \left(c^{-1}\right)^{20/9} \approx \frac{1}{4} X \tag{12}$$

at least to within around 10-15%, depending on the Reynolds number, X.

To validate this overlap argument, we also applied it to predict the optimal phase speed for skin friction modification reported in Kaithakkal et al. [18] for the travelling wave channel flow problem. The details of the calculation are presented in Appendix A, but the result is that for fixed wavelength, an optimal phase speed between 0.75 and 1.5 (non-dimensionalized with respect to the bulk channel velocity, $\hat{U}_b$) is expected, with only a weak Reynolds number dependence, exactly consistent with the reported findings. Thus the overlap argument appears to provide a robust method for optimizing the phase speed of forcing to enhance skin friction in both channel and boundary layer geometries.

However, Kaithakkal et al. [18] showed an optimum phase speed not only in the case of momentum flux, but also in the case of heat transfer modification, in contrast to the current study. Thus our original question regarding the apparent absence of an optimal phase speed for heat transfer in the boundary layer is twofold: why an optimum for heat transfer does not appear in the boundary layer in contrast to the skin friction, and why an optimum in heat transfer does appear in the case of a channel flow with wall-forcing?

3.3. Absence of optimal c for boundary layer heat flux

As noted above, the overall magnitude of the heat transfer modification is much larger than the skin friction modification, which indicates that the heat flux enhancement is not merely a consequence of advection via the velocity fluctuations, but rather involves additional interaction effects between the velocity and temperature fluctuations captured in the temperature forcing term, $f_\Theta(X, Y)$. We can verify this by neglecting the forcing term in the mean thermal dynamics equation, (5),

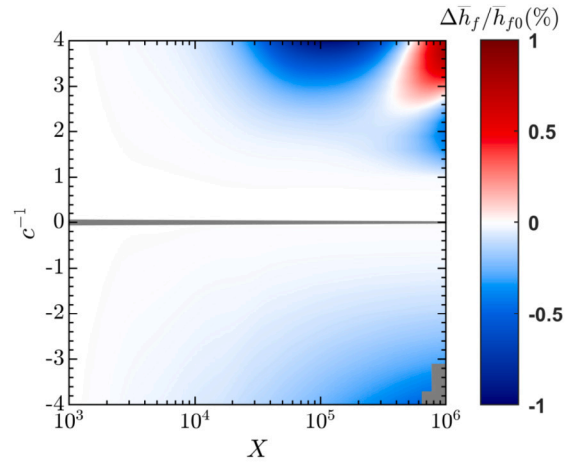

Fig. 4. Relative change in heat transfer coefficient, considering only momentum streaming and neglecting thermal forcing, as a function of Reynolds number (X) and inverse phase speed (c^{-1}), for (ϵ, Re_1, Pr) = (0.01, 2×10^4, 0.71).

and calculating the resulting heat transfer modification without forcing, shown in Fig. 4.

Without the forcing term, the magnitude of the heat transfer modification becomes much smaller but an optimal phase speed appears for the heat transfer, as it did for the momentum transfer. Indeed, the overall pattern of heat flux enhancement without the forcing, shown in Fig. 4, looks remarkably similar to the skin friction enhancement shown in Fig. 2. This indicates that the forcing, f_Θ, is responsible for both the higher overall amplification of the heat flux and the seeming disappearance of an optimal phase speed.

Thus, it is conceivable that an optimal phase speed for heat transfer exists even with the forcing included, but that it is obscured by the overall increase more broadly and might not be visible until higher X, as the boundary layer grows more and the critical and Stokes layers separate more, thus narrowing the range of phase speeds which result in an effective overlap of layers. (For low X, and finite critical layer thickness, a potentially wide range of phase speeds can all result in overlapping viscous layers.) This would also explain why an optimal phase speed for heat transfer is visible for the channel flow experiments: those flows are assumed fully developed, and thus, even at lower Reynolds numbers, the separate layers are established in discrete locations associated with only a narrow range of phase speeds. (The Reynolds number difference between the channel and boundary layer flows is quite significant, by nearly an order of magnitude in the region where the optimal phase speeds are most apparent in the boundary layer, as summarized in Table 1.)

The effect of the momentum and thermal forcing terms can also be visualized in terms of the resulting mode shapes of velocity and temperature fluctuations. Fig. 5 shows shapes of temporal fluctuating modes for both components of velocity and temperature. The near-wall phase of temperature fluctuations is completely different from the stream-wise velocity fluctuations, the reason for which can be ascribed to thermal forcing, since without the forcing, the temperature fluctuations would be passively advected and thus entirely in-phase with the velocity.

It is also worth recalling that the momentum forcing term, $f(X, Y)$, represents non-linear interactions between the velocity components, whereas the thermal forcing term, f_Θ, represents linear interactions with respect to temperature. The nature of the interaction will then affect the resulting phase of the different fluctuating modes, and the resulting amplitude of their combined effect in the forcing term (as it does in the classic Stokes problem – see Panton [23]).

Finally, the absence of an optimal phase speed in the current problem may be related to the use of free-stream forcing, which differs significantly from the wall forcing used in Kaithakkal et al. [18], where the forcing was imposed in a varicose mode, which may affect the crit-

Table 1
Range of non-dimensional parameters for the laminar boundary layer calculation as compared to the channel flow study of Kaithakkal et al. [18]. Re_δ is the Reynolds number defined in term of the boundary layer thickness, δ_{99}.

	ε	λ_x	c^{-1}	X	Pr
Kaithakkal et al. [18]	0.15	$2\pi/5 \sim 4\pi$	$-3.3 \sim 3.3$	$Re_H = 10, 100, 500$	1
Current (Boundary Layer)	0.01	$2\pi \sim \infty$	$-4 \sim 4$	$Re_\delta < 5 \times 10^3$	0.5, 0.71, 1

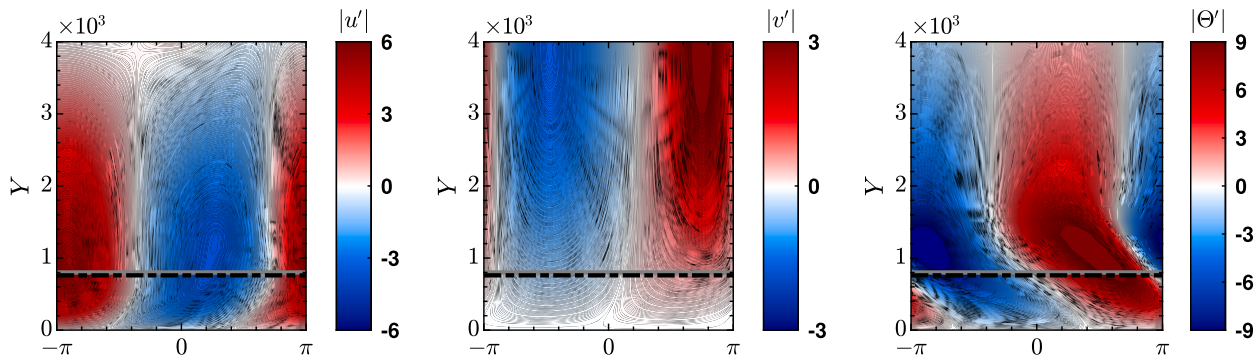

Fig. 5. Non-dimensional streamwise velocity (u'), wall normal velocity (v') and temperature (Θ') fluctuating temporal modes for (ε, Re_1, c^{-1}, X, Pr) = (0.01, 2×10^4, 4, 10^6, 0.71). The solid grey line represents the Stokes layer, Y_s, and the dashed black line represents the critical layer location, Y_c.

ical layer dynamics differently than center-line forcing would, besides any direct influence from the wall suction and blowing.

3.4. Scaling with Prandtl number

In our previous study on skin friction effects, the variation of fluctuation amplitude was analyzed as a function of forcing amplitude, ε, and streaming Reynolds number, Re_1. The same scaling with respect to these two variables holds for the thermal transport in the current study, as well. Additionally, we analyzed the heat flux modification with respect to changes in the Prandtl number over a limited range of practical engineering concern. Increasing the value of Pr increases the amplitude of temperature fluctuations as shown in Fig. 6(a), and this increase scales with $\sqrt{\mathrm{Pr}}$ as shown in Fig. 6(b), although the reason for this scaling has not been established. The fluctuating temperature dynamics equation, (7), would seem to suggest scaling with Pr instead. The wall-normal location of the peak amplitude does not change with Pr, which indicates no Prandtl number dependence in the characteristic length scales of temperature fluctuations in the wall normal direction.

As opposed to the temperature fluctuations, the Prandtl number dependence of the mean heat flux modification does appear linear, as expected from the mean dynamics, (5), and shown in Fig. 7. The difference between the Prandtl dependence in the fluctuations and mean flux is associated with the phase of the fluctuating modes themselves. The phase of temperature fluctuations near the wall was found to decrease linearly from 3.3 to 2.5 radians for Pr variation from 0.5 to 1. This change in phase results in different forcing and thus different mean fluxes, meaning that the average flux will depend differently on Pr than the time-varying fluctuations themselves.

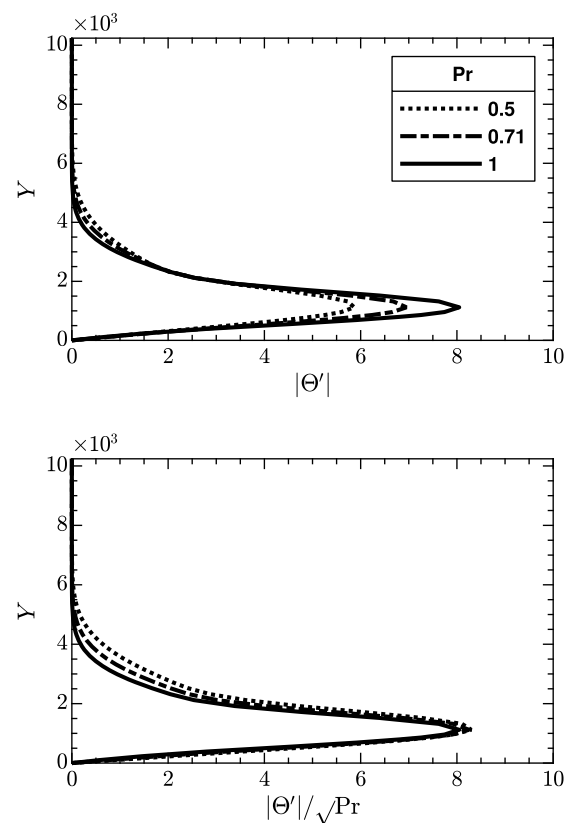

Fig. 6. Amplitude of temperature fluctuations as a function of wall normal distance (Y) for three different Pr, with (ε, Re_1, X, c^{-1}) = (0.01, 2×10^4, 7.7×10^5, 2.8).

4. Conclusions

Free-stream, traveling-wave velocity disturbances were introduced computationally to a laminar, thermal boundary layer in order to study their effect on the heat flux at the wall, and to compare the effect on the heat flux with that of the skin friction. The heat flux modification was substantially larger than the skin friction enhancement, and the overall dependence of that enhancement on the phase speed and streamwise location was significantly different. Unlike the skin friction, which showed an optimal phase speed at which the momentum flux at the wall was enhanced, the heat flux appeared to show a monotonic increase with phase speed.

The differences between the magnitudes of the thermal and momentum flux modifications were attributed to the nature of the forcing associated with the two systems: non-linear interactions of fluctuations

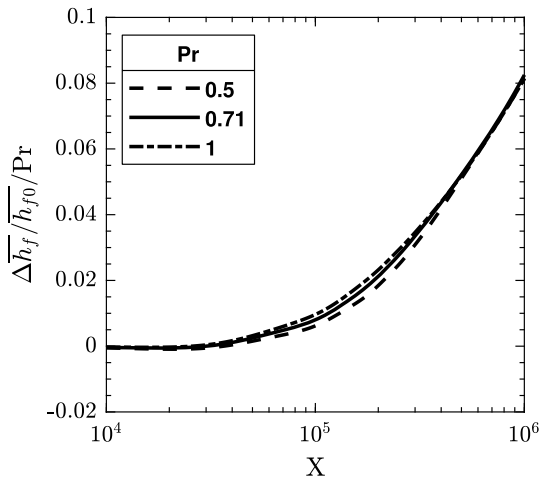

Fig. 7. Relative change in heat transfer coefficient divided by Prandtl number for different Prandtl numbers, as a function of Reynolds number (X), with (ε, Re_1, c^{-1}) = (0.01, 2×10^4, 2.8).

for momentum and linear-interactions of fluctuations for temperature, which result in vastly different phase profiles of the fluctuating modes, and thus different amplitudes for the forcing terms in the mean dynamics equations.

We also generalized the overlap argument used to predict the optimal phase speed for increased wall transport and validated it against previously published channel flow results for both thermal and momentum transport. We speculated on possible reasons for the absence of an optimal phase speed in the laminar boundary layer problem, including the possibility that an underlying optimum was obscured due to insufficient development of the boundary layer, and we calculated the thermal flux by neglecting the thermal forcing term in order to demonstrate evidence of an underlying optimum.

The present calculation of the thermal boundary layer exposed to free-stream velocity forcing provides a companion study to many of the classical reports of traveling wave forcing of laminar boundary layers, and demonstrates the significant effect that even small velocity perturbations can have on the measured heat flux, which has important implications for making heat flux measurements in unsteady environments contaminated by traveling wave perturbations.

CRediT authorship contribution statement

Tapish Agarwal: Investigation, Methodology, Software, Visualization, Writing – original draft. **Beni Cukurel:** Conceptualization, Methodology, Supervision, Writing – review & editing. **Ian Jacobi:** Formal analysis, Methodology, Supervision, Writing – original draft.

Declaration of competing interest

The authors declare that they have no known competing financial interests or personal relationships that could have appeared to influence the work reported in this paper.

Data availability

The data that support the findings of this study are available from the corresponding author, IJ, upon reasonable request.

Acknowledgements

The authors gratefully acknowledge the support of the European Research Council (ERC) under the European Union's Horizon 2020 Research and Innovation Programme (Grant Agreement No 853096, ThermoTON) and the Israel Science Foundation (Grant 219/21).

Appendix A. Channel flow optimal phase speed

As a validation of the proposed overlap argument, we applied the overlap calculation to determine the optimal phase speed for momentum and heat flux enhancement in the case of channel flow for fixed disturbance wavelength, as reported in figures 2(a-b) of Kaithakkal et al. [18]. We start with the non-dimensional wavelength,

$$\lambda = 2\pi c\frac{\mathrm{Re}_1}{\mathrm{Re}} = \mathrm{const} \tag{A.1}$$

where λ is $\hat{\lambda}/\hat{\ell}$ and we take Re to be defined with respect to the channel half-height, $\hat{H}$. Substituting the Stokes layer thickness, Y_s for the wavelength λ and then imposing the overlap criterion, $Y_s = Y_c$, we obtain:

$$\frac{\lambda\alpha_s^2}{2\pi} = \frac{cY_c^2}{\mathrm{Re}} = \mathrm{const} \tag{A.2}$$

Therefore, we substitute for Y_c in terms of the velocity profile to determine the value of the phase speed at which the amplification is expected to occur, based on our overlap argument. For standard Poiseuille flow in a channel from $(-H, +H)$, we can write the mean velocity profile as:

$$u = \frac{3}{2}\left[1 - \left(\frac{1}{\mathrm{Re}}\frac{Y}{H}\right)^2\right] \tag{A.3}$$

where u is non-dimensionalized with respect to the bulk velocity $\hat{U}_b$. Solving for Y and substituting for (Y_c, c), we obtain:

$$Y_c^2 = \mathrm{Re}^2\left(1 - \frac{2}{3}c\right) \tag{A.4}$$

Finally we substitute into the overlap relation for fixed wavelength, $cY_c^2/\mathrm{Re} = \mathrm{const}$, and solve for c yielding the optimal phase speed associated with the overlap of the critical and Stokes layers within the channel flow:

$$c = \frac{3}{4}\left[1 \pm \sqrt{1 - \frac{4\alpha_s^2}{3\pi}\frac{\lambda}{H}\mathrm{Re}^{-1}}\right] \tag{A.5}$$

To obtain real values of the phase speed in equation (A.5) (i.e. neutrally stable traveling waves), the phase speeds are limited between 3/2 and 3/4, i.e. between the centerline velocity and half the centerline velocity, for the upper (positive branch). If we choose the lower (negative branch), then the velocities are limited to 0 to 3/4, i.e. between the wall and half the centerline velocity. But we choose the upper branch since that indicates a distinct critical layer, distinct from the wall. Thus we would expect in this case phase speeds $\frac{3}{4} < c < \frac{3}{2}$, which is consistent with figure 2(a-b) of Kaithakkal et al. [18]. The complex solutions to this quadratic expression reflect non-neutrally stable traveling wave solutions, but their real parts remain bounded as above.

References

[1] R.C. Ackerberg, J.H. Phillips, The unsteady laminar boundary layer on a semi-infinite flat plate due to small fluctuations in the magnitude of the free-stream velocity, J. Fluid Mech. 51 (1972) 137–157, https://doi.org/10.1017/S0022112072001119.

[2] T. Agarwal, B. Cukurel, I. Jacobi, Localized drag modification in a laminar boundary layer subject to free-stream travelling waves via critical and Stokes layer interactions, J. Fluid Mech. 937 (2022) A10, https://doi.org/10.1017/S0022112085001276.

[3] A.A. Ameri, D.L. Rigby, E. Steinthorsson, J. Heidmann, J.C. Fabian, Unsteady analysis of blade and tip heat transfer as influenced by the upstream momentum and thermal wakes, https://doi.org/10.1115/GT2008-51242, 2008, pp. 1095–1103.

[4] L.N. Cattafesta, M. Sheplak, Actuators for active flow control, Annu. Rev. Fluid Mech. 43 (2011) 247–272, https://doi.org/10.1146/annurev-fluid-122109-160634.

[5] J. Choi, Role of Free-Surface Boundary Conditions and Nonlinearities in Wave/Boundary-Layer and Wake Interaction, Ph.D. thesis, The University of Iowa, 1993.

[6] J.E. Choi, M.K. Sreedhar, F. Stern, Stokes layers in horizontal-wave outer flows, J. Fluids Eng. 118 (1996) 537–545, https://doi.org/10.1115/1.2817792.

[7] J.E. Choi, F. Stern, Solid fluid juncture boundary layer and wake with waves, in: Proceedings of the Sixth International Conference on Numerical Ship Hydrodynamics, 1993, pp. 1–50.

[8] R.L. Evans, Computation of unsteady laminar boundary layers subject to traveling-wave freestream fluctuations, AIAA J. 27 (1989) 1644–1646, https://doi.org/10.2514/3.10313.
[9] S. Gendebien, A. Kleiman, B. Leizeronok, B. Cukurel, Experimental investigation of forced convection enhancement by acoustic resonance excitations in turbulated heat exchangers, J. Turbomach. 142 (2) (2020) 021005 (9 pages), https://doi.org/10.1115/1.4045659.
[10] J.C. Han, L. Zhang, S. Ou, Influence of unsteady wake on heat transfer coefficient from a gas turbine blade, J. Heat Transf. 115 (1993) 904–911, https://doi.org/10.1115/1.2911386.
[11] Y. Hasegawa, N. Kasagi, Dissimilar control of momentum and heat transfer in a fully developed turbulent channel flow, J. Fluid Mech. 683 (2011) 57–93, https://doi.org/10.1017/jfm.2011.248.
[12] K. Higashi, H. Mamori, K. Fukagata, Simultaneous control of friction drag reduction and heat transfer augmentation by traveling wave-like blowing/suction, Comput. Therm. Sci. Int. J. 3 (2011) 521–530.
[13] P.G. Hill, A.H. Stenning, Laminar boundary layers in oscillatory flow, J. Basic Eng. 82 (1960) 593–607, https://doi.org/10.1115/1.3662672.
[14] C. Ho, P. Huerre, Perturbed free shear layers, Annu. Rev. Fluid Mech. 16 (1984) 365–422, https://doi.org/10.1146/annurev.fl.16.010184.002053.
[15] J. Hoepffner, K. Fukagata, Pumping or drag reduction?, J. Fluid Mech. 635 (2009) 171–187, https://doi.org/10.1017/S0022112009007629.
[16] S. Jiang, Z. Li, J. Li, Effect of unsteady passing wake on the aerodynamic and heat transfer performance of the turbine blade squealer tip, Proc. Inst. Mech. Eng. A, J. Power Energy 237 (2023) 19–32, https://doi.org/10.1177/09576509221104571.
[17] A.J. Kaithakkal, Y. Kametani, Y. Hasegawa, Dissimilarity between turbulent heat and momentum transfer induced by a streamwise travelling wave of wall blowing and suction, J. Fluid Mech. 886 (2020) A29, https://doi.org/10.1017/jfm.2019.1045.
[18] A.J. Kaithakkal, Y. Kametani, Y. Hasegawa, Dissimilar heat transfer enhancement in a fully developed laminar channel flow subjected to a traveling wave-like wall blowing and suction, Int. J. Heat Mass Transf. 164 (2021) 120485, https://doi.org/10.1016/j.ijheatmasstransfer.2020.120485.
[19] P.M. Ligrani, M.M. Oliveira, T. Blaskovich, Comparison of heat transfer augmentation techniques, AIAA J. 41 (2003) 337–362, https://doi.org/10.2514/2.1964.
[20] C. Lin, Motion in the boundary layer with a rapidly oscillating external flow, in: 9th International Congress of Applied Mechanics, 1957.
[21] H. Mamori, K. Fukagata, J. Hoepffner, Phase relationship in laminar channel flow controlled by traveling-wave-like blowing or suction, Phys. Rev. E 81 (2010) 046304, https://doi.org/10.1103/PhysRevE.81.046304.
[22] R. Nickerson, The Effect of Free Stream Oscillations on the Laminar Boundary Layers on a Flat Plate, Ph.D. thesis, Massachusetts Institute of Technology, 1957.
[23] R.L. Panton, Incompressible Flow, 4 ed., John Wiley & Sons, 2013.
[24] M.H. Patel, On laminar boundary layers in oscillatory flow, Proc. R. Soc. A, Math. Phys. Eng. Sci. 347 (1975) 99–123, https://doi.org/10.1098/rspa.1975.0200.
[25] M.H. Patel, A.D. Young, On turbulent boundary layers in oscillatory flow, Proc. R. Soc. Lond. Ser. A, Math. Phys. Sci. 353 (1977) 121–144, https://doi.org/10.1098/rspa.1977.0025.
[26] N. Riley, Steady streaming, Annu. Rev. Fluid Mech. 33 (2001) 43–65.
[27] H. Schlichting, Amplitude distribution and energy balance of small disturbances in plate flow, Technical Report TM 1265, NACA, 1950.
[28] P. Schmid, D. Henningson, Stability and Transition in Shear Flows, vol. 1, Springer, 2000.
[29] M.T. Schobeiri, B. Öztürk, M. Kegalj, D. Bensing, On the physics of heat transfer and aerodynamic behavior of separated flow along a highly loaded low pressure turbine blade under periodic unsteady wake flow and varying of turbulence intensity, J. Heat Transf. 130 (2008), https://doi.org/10.1115/1.2885156.
[30] C. Sieverding, Recent progress in the understanding of basic aspects of secondary flows in turbine blade passages, J. Eng. Gas Turbines Power 107 (1985) 248–257.
[31] H.A. Siller, H.H. Fernholz, Manipulation of the reverse-flow region downstream of a fence by spanwise vortices, Eur. J. Mech. B, Fluids 26 (2007) 236–257, https://doi.org/10.1016/j.euromechflu.2006.05.005.
[32] J.T. Stuart, Double boundary layers in oscillatory viscous flow, J. Fluid Mech. 24 (1966) 673–687, https://doi.org/10.1017/S0022112066000910.
[33] D.P. Telionis, Unsteady Viscous Flow, Springer-Verlag, New York, 1981.
[34] D.P. Telionis, M.S. Romaniuk, Velocity and temperature streaming in oscillating boundary layers, AIAA J. 16 (1978) 488–495, https://doi.org/10.2514/3.60916.
[35] L. Wright, M.T. Schobeiri, The effect of periodic unsteady flow on aerodynamics and heat transfer on a curved surface, J. Heat Transf. 121 (1999) 22–33, https://doi.org/10.1115/1.2825954.
[36] L.M. Wright, Enhanced internal cooling of turbine blades and vanes, in: The Gas Turbine Handbook, U.S. Dept. of Energy-National Energy Technology Laboratory, 2006.